



# Versatile Dehydration-Assisted Functionalization of Quantum Dots and Rods

Chi Chen,\* Xin Luo, and Mark Bathe\*

**Abstract:** Functionalization of quantum dots (QDs) and quantum rods (QRs) with ligands is essential for their further practical application across various domains. Dehydration-assisted functionalization (DAF) is a versatile method applicable to a wide range of hydrophilic ligands with an affinity to the surface of QDs and QRs. This approach facilitates rapid one-pot ligand exchange and dense modification by efficiently transferring these ligands onto the surface of QDs and QRs. This study demonstrates the efficacy of DAF in preparing chiral QRs, engineering the surface charge of QDs, utilizing QR aggregates, and conjugating dense DNA onto cadmium-free InP/ZnS QDs. DAF therefore offers a versatile solution for hydrophilic ligand functionalization of QDs and QRs applicable to diverse applications.

Quantum dots (QDs) and quantum rods (QRs) have unique optical and electronic properties, including size-dependent band gaps, narrow emission spectra, tunable surface chemistry and charge transport, making them candidates for numerous applications in the field of display and lighting, lasing, and sensing.<sup>[1]</sup> Hydrophilic QDs and QRs hold particular significance because they enable the attachment of biomolecules such as DNA, peptides, and proteins onto the surface of these nanomaterials, opening up avenues for diverse *in vitro* and *in vivo* applications, including specific targeting and detection.<sup>[2]</sup> However, high-quality QD and QR production requires synthesis in organic

solvent with hydrophobic ligands, and the change of surface ligand is needed for hydrophilic functionalization.

Currently, mainstream methods for hydrophilic functionalization of QDs and QRs can be broadly classified into two categories: encapsulation, which involves direct addition of polymers, phospholipids, or silica to the hydrophobic ligand periphery; and ligand exchange, where hydrophilic ligands replace hydrophobic ones, followed by conjugation of functionalization groups in aqueous solution.<sup>[3]</sup> In the former strategy, dispersed QDs and QRs often exhibit larger hydrodynamic diameters due to additional material coating. While the latter approach typically yields more compact structures, ensuring sufficient surface coverage often requires significant incubation time or high temperatures, depending on the type of ligands used. For example, to modify QDs and QRs with single-stranded DNA (ssDNA) with a certain surface coverage, methods such as salt aging for several days<sup>[4]</sup> or shell growth at high temperature (90 °C)<sup>[5]</sup> may be required.

Recently, we demonstrated that dehydration-assisted DNA conjugation enables rapid ligand exchange and dense DNA modification directly with QDs and QRs dispersed in organic solvent such as toluene, hexane, and chloroform at room temperature in several minutes.<sup>[6]</sup> Utilizing these densely DNA conjugated cadmium-based QDs and QRs, we constructed QD/QR 2D arrays on 2D DNA origami superlattices.<sup>[6]</sup> However, we only investigated the application of this method for ssDNA functionalization. Here, we generalize this method to other ligands and QDs.

In this study, we identified dehydration-assisted functionalization (DAF) as a versatile and straightforward method applicable to diverse hydrophilic ligand exhibiting affinity to the surfaces of QDs and QRs, such as L-cysteine (L-Cys), D-cysteine (D-Cys), 3-mercaptopropionic acid (MPA), O-(2-mercaptoethyl)-O'-methyl-hexa(ethylene glycol) (mPEG), and thiol-modified ssDNA (Scheme 1). This method rapidly achieved ligand exchange and dense modification by efficiently condensing these ligands onto the surface of QDs and QRs followed by accelerated ligand anchorage. Leveraging DAF, we successfully prepared chiral QRs using L-Cys and D-Cys ligands, engineered the surface charge of QDs using dual-ligands comprising various ratios of MPA and mPEG, demonstrated the full utilization of QR aggregates, and achieved dense DNA conjugation on cadmium-free InP/ZnS QDs.

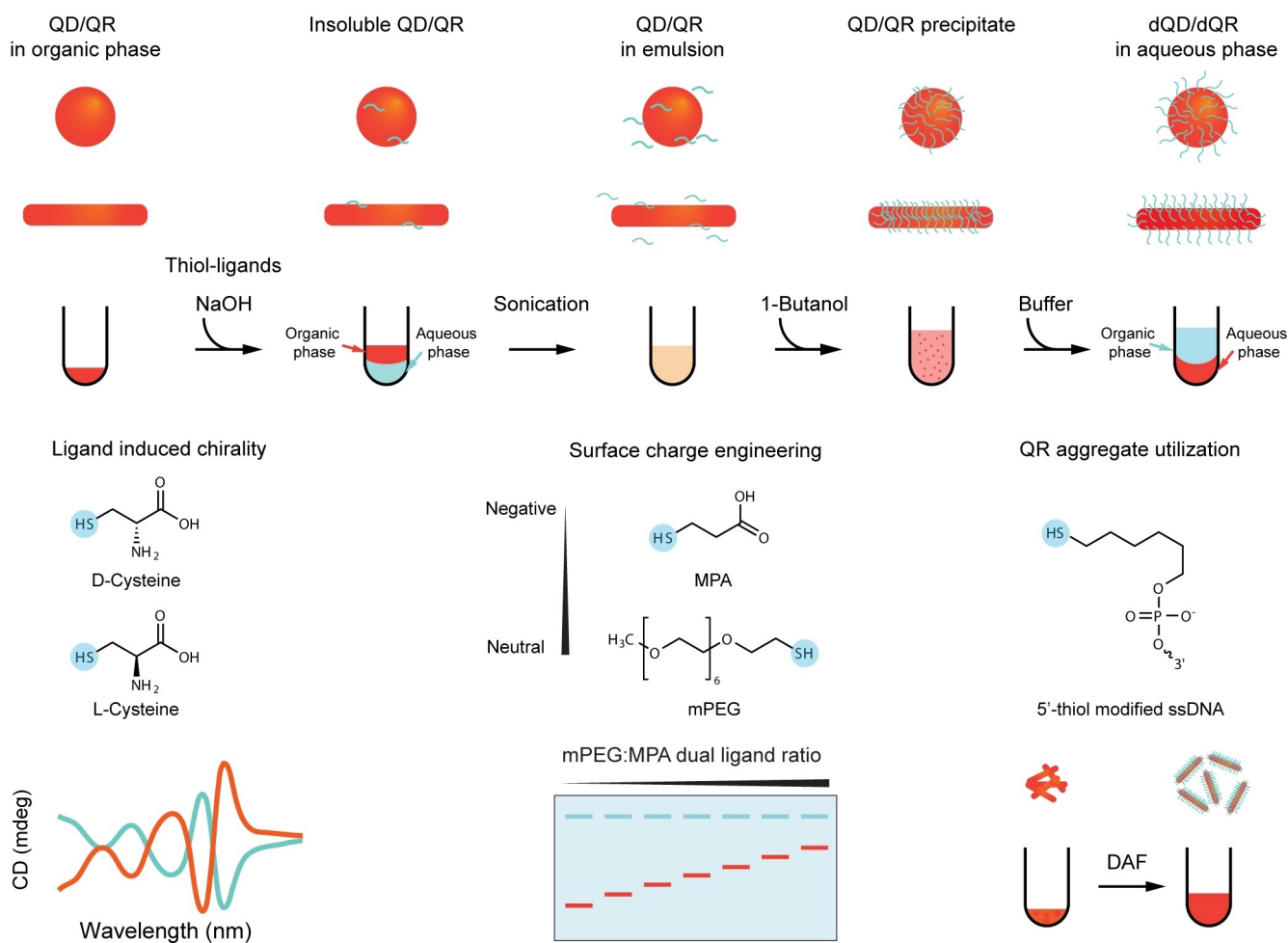
The optical activity of chiral QDs and QRs stems from surface chiral molecules, offering various applications in biology, chemistry, and physics.<sup>[7]</sup> Examples include site-selective photoinduced cleavage and profiling of DNA,<sup>[8]</sup>

[\*] Prof. C. Chen, Dr. X. Luo, Prof. M. Bathe  
 Department of Biological Engineering  
 Massachusetts Institute of Technology  
 Cambridge, MA, 02139, USA  
 E-mail: chi.chen@siat.ac.cn  
 mark.bathe@mit.edu

Dr. X. Luo  
 Department of Materials Science and Engineering  
 Massachusetts Institute of Technology  
 Cambridge, MA, 02139, USA

Prof. C. Chen  
 Shenzhen Institutes of Advanced Technology, Chinese Academy of Sciences  
 Shenzhen 518055, P. R. China

© 2024 The Authors. Angewandte Chemie International Edition published by Wiley-VCH GmbH. This is an open access article under the terms of the Creative Commons Attribution License, which permits use, distribution and reproduction in any medium, provided the original work is properly cited.



**Scheme 1.** Schematic of workflow and capabilities of the dehydration-assisted functionalization (DAF) strategy for QDs/QRs.

protein catalysis,<sup>[9]</sup> and spin-selective charge transport.<sup>[10]</sup> Conventional methods for preparing chiral QDs and QRs through phase transfer often require several tens of hours.<sup>[11–13]</sup> To demonstrate the rapid preparation of chiral QDs and QRs using DAF, we employed L-Cys and D-Cys to modify CdSe/CdS Dot-in-Rod emitting at 620 nm (QR620), and CdSe/ZnS QD emitting at 620 nm (QD620). Figure 1 shows the circular dichroism (CD) spectra of QR620 modified with L-Cys (dQR620-L-Cys) and D-Cys (dQR620-D-Cys) obtained from the organic solvent using DAF, which required only several minutes. The data indicate that the ligand imprinted its chirality onto the excitonic transitions of the QRs, distinct from the intense CD signal of cysteine in the ultraviolet region of the spectrum.<sup>[14,15]</sup> This strong CD signal at the absorption wavelength can be attributed to the transition of linearly polarized excitons in the QRs.<sup>[16]</sup> In contrast, almost no signal was observed for dQD620-L-Cys or dQD620-D-Cys, possibly due to a barrier effect of the wide band gap ZnS shell structure,<sup>[17]</sup> as most examples of ligand-induced chirality have involved the use of CdE (E = S, Se, Te) cores.<sup>[10–12,18,19]</sup> Another possible explanation is that the high curvature of QDs leads to adjacent ligands chelating in

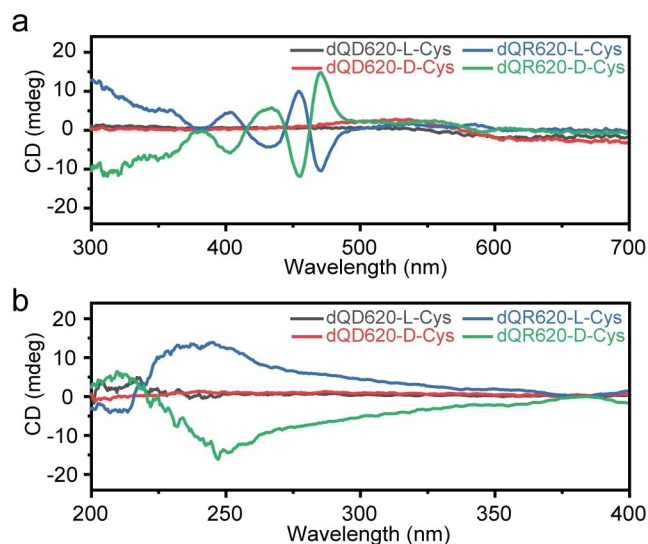


**Figure 1.** Introducing chirality to QDs and QRs using DAF. CD spectra of the QD620-L-Cys, QD620-D-Cys, QR620-L-Cys and QR620-D-Cys at a) visible and b) UV band.

opposite orientations, affecting the CD response and resulting in a weak CD signal.<sup>[19]</sup> Computational studies have suggested that CdSe CD spectra are highly sensitive to the structure of the ligand shell, as adjacent ligands can chelate in either *cis* or *trans* orientations, thereby influencing the CD response.<sup>[18]</sup> Quantitative analysis of the CD peaks is further conducted by calculating and comparing their anisotropic *g*-factor (Figure S1). The highest *g*-factor magnitude ( $g_{CD}$ ), defined as  $|g_{CD-} - g_{CD+}|/2$ , serves as an indicator of the magnitude of the induced chirality of dQR620.<sup>[20]</sup> We observed a  $g_{CD}$  of  $5.3 \times 10^{-4}$  and  $5.9 \times 10^{-4}$  for dQR620-L-Cys and dQR620-D-Cys, respectively (Table S1), consistent with those reported in literature for Cys-modified QRs with a similar core diameter, shell thickness, and aspect ratio prepared using traditional phase transfer methods.<sup>[21]</sup> Thus, DAF enables the rapid preparation of chiral QRs with a similar *g*-factor.

Dual-ligand modification of QDs and QRs has demonstrated important multifunctionality. For example, utilizing both photocrosslinkable ligand and dispersing ligand rendered QDs compatible with solution-based patterning techniques.<sup>[22]</sup> For QD-sensitized solar cells, incorporating MPA and inorganic ligands reduces the solvation free energy and facilitates QD loading, while also suppressing defect trap states,<sup>[23]</sup> enhancing optoelectronic performance.<sup>[23]</sup> However, an outstanding challenge remains the control over the ratio of dual-ligands on the surfaces of QDs and QRs.

Given that the DAF process condenses most initial aqueous ligands instantaneously onto QDs and QRs, we hypothesized that it is capable of controlling the ratio of different ligands on the QD surface, by adjusting initial ligand stoichiometry used in the functionalization process. We selected the small molecule thiol ligands MPA and mPEG to test this hypothesis, because we can easily characterize the dual-ligand ratio based on QD surface charge, as MPA carries a negative charge and mPEG is neutral. By mixing the two ligands in varying proportions for DAF (9:1, 8:2, 7:3, 6:4, 5:5, 4:6, 3:7, 2:8, 1:9), we obtained QDs with nine different dual-ligand ratios (Figure 2a). Spectroscopic analysis revealed negligible changes in absorption and emission spectra of dQD620 with dual-ligands, with quantum yields mostly ranging between 5–20% (Figure S2). Agarose gel electrophoresis (AGE) demonstrated distinct band mobilities, indicating controlled QD surface charges engineered via dual-ligand ratios (Figure 2b and Figure S3). Further analysis of hydrodynamic diameters using dynamic light scattering (DLS) revealed MPA-only-modified QDs to be smaller at 8.3 nm, while other hydrodynamic diameters increased slightly to 11.2 nm with the rise in mPEG proportion (Figure S4). Zeta potential measurements confirmed this, with average zeta potentials decreased from  $-35.0 \pm 2.9$  to  $-5.4 \pm 0.6$  mV (mean  $\pm$  standard deviation;  $n=3$ ) as less MPA ligand were incorporated (Figure 2c). Thus, the DAF method enabled the rapid preparation of seven distinct surface-charged QDs within minutes (Figure S4). In addition, surface charge of QDs can influence both the kinetics of the phosphorothioate backbone (ps-backbone) ssDNA wrapping and the resulting

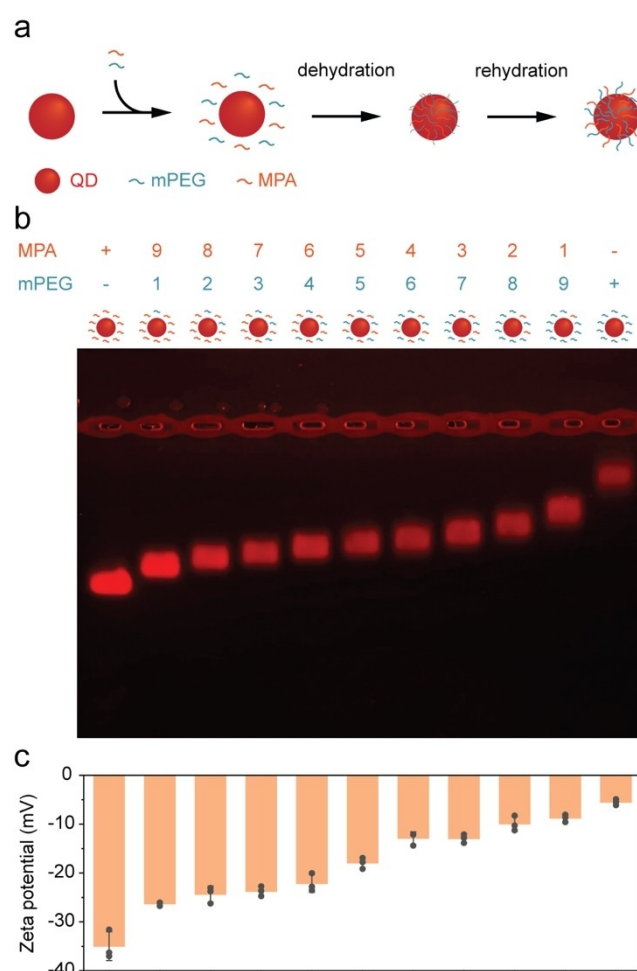


**Figure 2.** Surface charge engineering of dQD620 with dual-ligands using DAF. a) Schematic of dual-ligand functionalization of QDs b) AGE gel images of dual-ligand modified dQD620 with different MPA and mPEG ratios (+ and - indicate the presence and absence of ligands, respectively). c) Corresponding average zeta potential results at pH=8.0. Error bars in c) represent standard deviation of the mean ( $n=3$  replicates per group).

spatial conformation.<sup>[24]</sup> The ability to modulate the surface charge of QDs enables the valence control using DNA complexes<sup>[25]</sup> and geocoding of ssDNA valence on the QD surface using wireframe DNA origami.<sup>[26]</sup> However, existing methods require a four-day incubation of MPA-modified QDs with mPEG to neutralize the negative charge before ssDNA wrapping, with no effective strategies to control the dual-ligand ratio on the QD surface, thereby hindering surface charge engineering.<sup>[25,26]</sup>

Nanowaste is a growing global safety concern, underscoring the need for precise environmental waste management and regulation.<sup>[27]</sup> According to estimates, up to 20% of all nanomaterials waste comes from research institutions,<sup>[28]</sup> highlighting the importance to fully utilize nanomaterials to reduce waste disposal, particularly those that are toxic to humans and the environment such as cadmium, lead, mercury-containing QDs and QRs. Considering the versatile ligand-conjugation capability of the DAF

method, we attempted to utilize this approach for ligand exchange and utilization of aggregated QRs, in order to reduce nanowaste. Specifically, we observed that commercially available QRs functionalized with oleic acid (OA) tended to aggregate significantly in their initial hexane solution during storage overtime, with aggregation typically occurring within a few months, which renders these materials unusable. Additionally, QRs are typically in limited supply commercially, needing to be synthesized upon receiving orders, further highlighting their challenging storage characteristics. Thus, if the DAF method could be used for the utilization of aggregated QRs, it would lead to substantial cost savings as well as significant reduction in

waste, thereby promoting sustainability. Consequently, we attempted to test the modification of aggregated OA modified QRs emitting at 620 nm (QR620ag-OA) with hydrophilic ligands by dispersing them into aqueous buffer using DAF (Figure 3a and Figure S5).

We characterized the particle size distribution in solution using multi-angle dynamic light scattering (MADLS). To avoid interference from the purification-centrifugation process, samples were measured immediately after DAF. For QR620ag-OA, we observed that the majority of the aggregate particle sizes were greater than 1000 nm (Figure 3b). We presumed that this aggregation was due to the detachment of OA ligands. Thus, we attempted to redis-

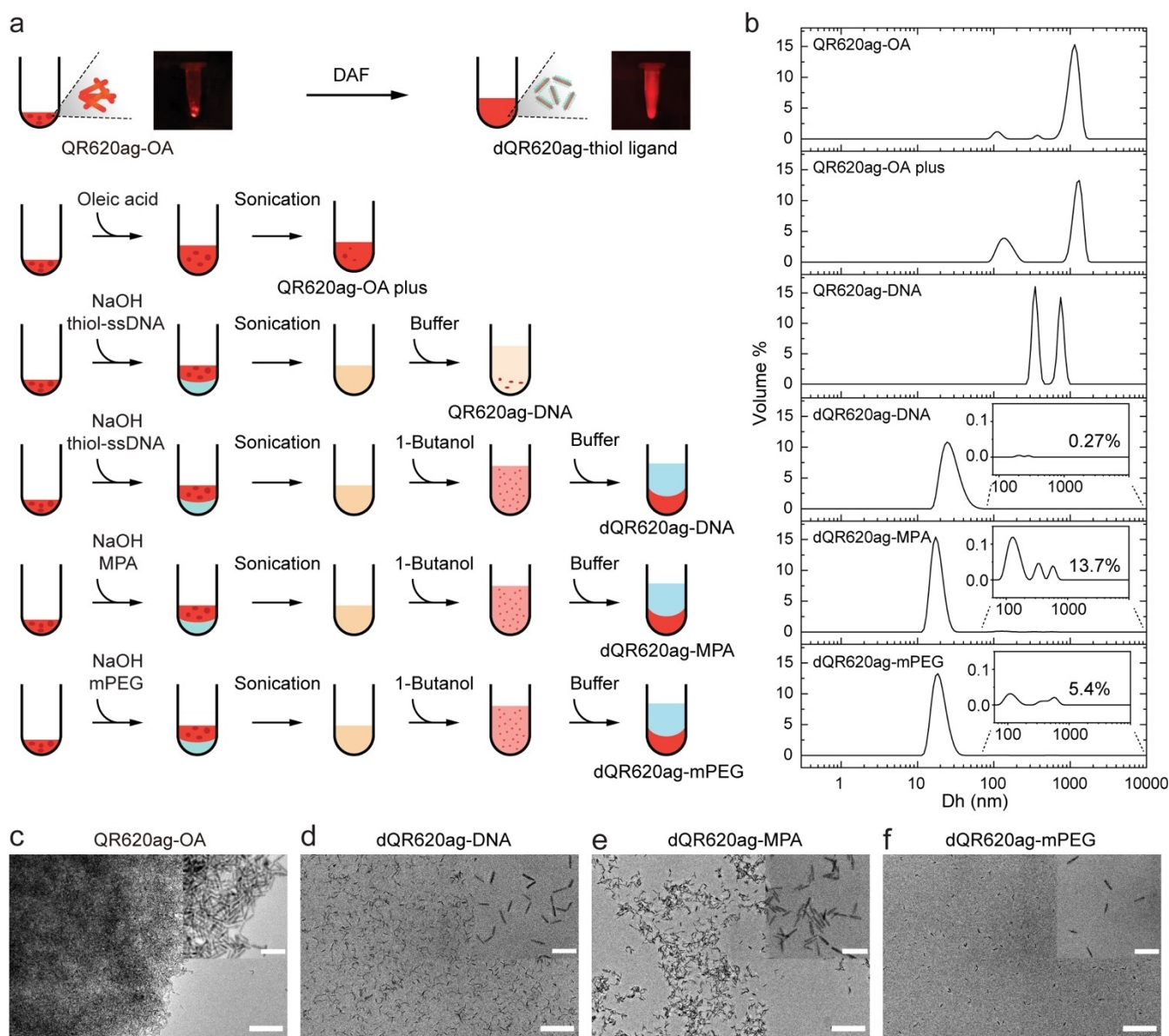


**Figure 3.** QR aggregates utilization using DAF. a) Schematic of QR aggregates utilization. b) MADLS measurement showing the size distribution of QR620ag-OA, QR620ag-OA plus, QR620ag-DNA, dQR620ag-DNA, dQR620ag-MPA, and dQR620ag-mPEG. Inset: zoomed region for the 100–1000 nm scale. c) Representative wide-field and high-resolution TEM images of QR620ag-OA, dQR620ag-DNA, dQR620ag-MPA, and dQR620ag-mPEG (Scale bar: 200 nm for c–f, 50 nm for inset).

perse QR620ag-OA by adding additional OA ligands and performing ultrasonication (QR620ag-OA plus). While a slight decrease was observed in the proportion of aggregate particle around 1000 nm in size with a slight increase in the proportion of those around 100 nm in size, we were unable to achieve monodisperse QRs using this method (Figure 3b). In contrast, we obtained monodisperse QRs using the DAF method with three different thiol ligands, including thiolated-ssDNA (dQR620ag-DNA), MPA (dQR620ag-MPA), and mPEG (dQR620ag-mPEG) (Figure 3b). In the section ranging from 100 to 10,000 nm, the remaining percentages of dQR620ag-ssDNA, dQR620ag-MPA, dQR620ag-mPEG were 0.27 %, 13.7 %, and 5.4 %, respectively (Figure 3b inset). However, using only ultrasonication to conjugate thiolated-ssDNA (without butanol dehydration) resulted in a turbid solution with particle sizes distributed between 200 and 2000 nanometers. Wide-field and high-resolution TEM images further confirmed our conclusion (Figure 3c–3f and Figure S6–S9).

The DAF method only requires mild conditions and is easily scalable for production (Figure S10). DAF-QD and DAF-QR also demonstrated excellent photoluminescence intensity stability in buffers of various pH (Figure S11). When stored at higher concentrations (1  $\mu$ M for QD, 100 nM for QR), DAF-QD and DAF-QR maintained colloidal stability (no aggregation) after more than three months of storage at 4 °C in 10 mM Tris buffer (pH 8.0). Importantly, it is not limited to cadmium-based QDs; it also applies to InP/ZnS QDs emission at 650 nm (InP650) in the presence of tris(2-carboxyethyl)phosphine (TCEP), consistent with the previously reported aqueous phase transfer method for InP/ZnS QDs (Figure S12).<sup>[29]</sup> Furthermore, the DNA density on InP650 was similar to our previously reported value for CdSe/ZnS QDs using DAF (Table S2).<sup>[6]</sup> This consistency is crucial for the broad application of large-scale, non-toxic QDs.

In conclusion, DAF is a rapid, straightforward, and efficient one-pot method for phase transfer and hydrophilic functionalization of QDs synthesized in organic solvents. Currently, we have only validated this method for different hydrophilic ligands with mono-thiol anchoring groups. Theoretically, this method can be applied to any hydrophilic ligand that has sufficient affinity for the QD/QR surface. For example, polydentate thiolated ligands can be employed to improve long-term stability,<sup>[30]</sup> polyhistidine tags can be employed to conjugate peptides and proteins,<sup>[31]</sup> and ps-backbone ssDNA<sup>[26]</sup> can be investigated for controllable ligand valency. We believe that DAF's capabilities such as rapid ligand exchange, dual-ligand functionalization with precise tuning of stoichiometric ratios, and the ability to fully utilize QD and QR aggregates, will provide a versatile approach for hydrophilic ligand functionalization of QDs and QRs for diverse applications in nanoscience and nanotechnology.

## Acknowledgements

The authors thank MIT nano for its electron microscope facility (TEM) and Bio BIF for its Circular Dichroism Spectrometer. We are grateful for funding from the National Science Foundation CCF 1956054 and the Office of Naval Research N00014-21-1-4013.

## Conflict of Interest

C.C., X.L., and M.B. are co-inventors on a patent pending (U.S. Patent Application No. 63/485,855) submitted by MIT for the rapid and scalable solution-based fabrication of quantum dot and quantum rod 2D arrays using DNA origami.

## Data Availability Statement

The data that support the findings of this study are available from the corresponding author upon reasonable request.

**Keywords:** Functionalization · Phase transfer · Chirality · Dual-ligands · Aggregate

- [1] F. P. García de Arquer, D. V. Talapin, V. I. Klimov, Y. Arakawa, M. Bayer, E. H. Sargent, *Science* **2021**, *373*, eaaz8541.
- [2] K. D. Wegner, N. Hildebrandt, *Chem. Soc. Rev.* **2015**, *44*, 4792–4834.
- [3] A. Banerjee, T. Pons, N. Lequeux, B. Dubertret, *Interface Focus* **2016**, *6*, 20160064.
- [4] G. P. Mitchell, C. A. Mirkin, R. L. Letsinger, *J. Am. Chem. Soc.* **1999**, *121*, 8122–8123.
- [5] Z. Deng, A. Samanta, J. Nangreave, H. Yan, Y. Liu, *J. Am. Chem. Soc.* **2012**, *134*, 17424–17427.
- [6] C. Chen, X. Luo, A. E. K. Kaplan, M. G. Bawendi, R. J. Macfarlane, M. Bathe, *Sci. Adv.* **2023**, *9*, eadh8508.
- [7] X. Gao, B. Han, X. Yang, Z. Tang, *J. Am. Chem. Soc.* **2019**, *141*, 13700–13707.
- [8] M. Sun, L. Xu, A. Qu, P. Zhao, T. Hao, W. Ma, C. Hao, X. Wen, F. M. Colombari, A. F. De Moura, N. A. Kotov, C. Xu, H. Kuang, *Nat. Chem.* **2018**, *10*, 821–830.
- [9] C. Hao, R. Gao, Y. Li, L. Xu, M. Sun, C. Xu, H. Kuang, *Angew. Chem. Int. Ed.* **2019**, *58*, 7371–7374.
- [10] B. P. Bloom, V. Kiran, V. Varade, R. Naaman, D. H. Waldeck, *Nano Lett.* **2016**, *16*, 4583–4589.
- [11] M. P. Moloney, J. Govan, A. Loudon, M. Mukhina, Y. K. Gun'ko, *Nat. Protoc.* **2015**, *10*, 558–573.
- [12] U. Tohgha, K. K. Deol, A. G. Porter, S. G. Bartko, J. K. Choi, B. M. Leonard, K. Varga, J. Kubelka, G. Muller, M. Balaz, *ACS Nano* **2013**, *7*, 11094–11102.
- [13] J. Hao, Y. Li, J. Miao, R. Liu, J. Li, H. Liu, Q. Wang, H. Liu, M.-H. Delville, T. He, K. Wang, X. Zhu, J. Cheng, *ACS Nano* **2020**, *14*, 10346–10358.
- [14] G. Li, X. Fei, H. Liu, J. Gao, J. Nie, Y. Wang, Z. Tian, C. He, J.-L. Wang, C. Ji, D. Oron, G. Yang, *ACS Nano* **2020**, *14*, 4196–4205.
- [15] J. Hao, Y. Li, X. Xu, F. Zhao, R. Pan, J. Li, H. Liu, K. Wang, J. Li, X. Zhu, M. Delville, M. Zhang, T. He, J. Cheng, *Adv. Mater. Technol.* **2020**, *5*, 2000138.

- [16] X. Gao, X. Zhang, K. Deng, B. Han, L. Zhao, M. Wu, L. Shi, J. Lv, Z. Tang, *J. Am. Chem. Soc.* **2017**, *139*, 8734–8739.
- [17] F. Purcell-Milton, A. K. Vishratina, V. A. Kuznetsova, A. Ryan, A. O. Orlova, Y. K. Gun'ko, *ACS Nano* **2017**, *11*, 9207–9214.
- [18] J. K. Choi, B. E. Haynie, U. Tohgha, L. Pap, K. W. Elliott, B. M. Leonard, S. V. Dzyuba, K. Varga, J. Kubelka, M. Balaz, *ACS Nano* **2016**, *10*, 3809–3815.
- [19] B. P. Bloom, B. M. Graff, S. Ghosh, D. N. Beratan, D. H. Waldeck, *J. Am. Chem. Soc.* **2017**, *139*, 9038–9043.
- [20] J. Cheng, J. Hao, H. Liu, J. Li, J. Li, X. Zhu, X. Lin, K. Wang, T. He, *ACS Nano* **2018**, *12*, 5341–5350.
- [21] J. Hao, J. Li, M. Chen, X. Duan, B. Xu, Y. Li, T. He, X. W. Sun, M.-H. Delville, J. Cheng, *Mater. Chem. Front.* **2022**, *6*, 1194–1208.
- [22] D. Hahm, J. Lim, H. Kim, J.-W. Shin, S. Hwang, S. Rhee, J. H. Chang, J. Yang, C. H. Lim, H. Jo, B. Choi, N. S. Cho, Y.-S. Park, D. C. Lee, E. Hwang, S. Chung, C. Kang, M. S. Kang, W. K. Bae, *Nat. Nanotechnol.* **2022**, *17*, 952–958.
- [23] Z. Zhang, H. Song, W. Wang, H. Rao, Y. Fang, Z. Pan, X. Zhong, *ACS Energy Lett.* **2023**, *8*, 647–656.
- [24] X. Wei, C. Chen, Y. Zhao, E. Harazinska, M. Bathe, R. Hernandez, *ACS Nano* **2022**, *16*, 6666–6675.
- [25] J. Shen, Q. Tang, L. Li, J. Li, X. Zuo, X. Qu, H. Pei, L. Wang, C. Fan, *Angew. Chem. Int. Ed.* **2017**, *56*, 16077–16081.
- [26] C. Chen, X. Wei, M. F. Parsons, J. Guo, J. L. Banal, Y. Zhao, M. N. Scott, G. S. Schlau-Cohen, R. Hernandez, M. Bathe, *Nat. Commun.* **2022**, *13*, 4935.
- [27] F. Schwab, B. Rothen-Rutishauser, A. Scherz, T. Meyer, B. B. Karakoçak, A. Petri-Fink, *Nat. Nanotechnol.* **2023**, *18*, 317–321.
- [28] A. A. Keller, S. McFerran, A. Lazareva, S. Suh, *J. Nanopart. Res.* **2013**, *15*, 1692.
- [29] S. Tamang, G. Beaune, I. Texier, P. Reiss, *ACS Nano* **2011**, *5*, 9392–9402.
- [30] I. L. Medintz, H. T. Uyeda, E. R. Goldman, H. Mattoussi, *Nat. Mater.* **2005**, *4*, 435–446.
- [31] K. E. Sapsford, T. Pons, I. L. Medintz, S. Higashiya, F. M. Brunel, P. E. Dawson, H. Mattoussi, *J. Phys. Chem. C* **2007**, *111*, 11528–11538.
- [32] W. W. Yu, L. Qu, W. Guo, X. Peng, *Chem. Mater.* **2003**, *15*, 2854–2860.
- [33] E. Shaviv, A. Salant, U. Banin, *ChemPhysChem* **2009**, *10*, 1028–1031.
- [34] C. Würth, M. Grabolle, J. Pauli, M. Spieles, U. Resch-Genger, *Nat. Protoc.* **2013**, *8*, 1535–1550.

Manuscript received: May 30, 2024

Accepted manuscript online: July 19, 2024

Version of record online: September 5, 2024